Earth and Planetary Science Letters 289 (2010) 323–333

Contents lists available at ScienceDirect

Earth and Planetary Science Letters

journal homepage: www.elsevier.com/locate/epsl

Crustal intrusion beneath the Louisville hotspot track

E. Contreras-Reyes [a,b,*], I. Grevemeyer [a], A.B. Watts [c], L. Planert [a], E.R. Flueh [a], C. Peirce [d]

[a] IFM-GEOMAR, Leibniz-Institut für Meereswissenschaften, Wischhofstrasse 1-3, D-24148 Kiel, Germany
[b] Departamento de Geofísica, Universidad de Chile, Blanco Encalada 2002, Santiago, Chile
[c] Department of Earth Sciences, University of Oxford, Parks Road, Oxford OX1 3PR, UK
[d] Department of Earth Sciences, Durham University, South Road, Durham DH1 3LE, UK

ARTICLE INFO

Article history:
Received 24 February 2009
Received in revised form 7 October 2009
Accepted 8 November 2009
Available online 5 December 2009

Editor: R.D. van der Hilst

Keywords:
hotspots
Louisville Ridge
intrusion
crustal structure
gravity anomalies
flexure

ABSTRACT

We report here the first detailed 2D tomographic image of the crust and upper mantle structure of a Cretaceous seamount that formed during the interaction of the Pacific plate and the Louisville hotspot. Results show that at ~1.5 km beneath the seamount summit, the core of the volcanic edifice appears to be dominantly intrusive, with velocities faster than 6.5 km/s. The edifice overlies both high lower crustal (>7.2–7.6 km/s) and upper mantle (>8.3 km/s) velocities, suggesting that ultramafic rocks have been intruded as sills rather than underplated beneath the crust. The results suggest that the ratio between the volume of intra-crustal magmatic intrusion and extrusive volcanism is as high as ~4.5. In addition, the inversion of Moho reflections shows that the Pacific oceanic crust has been flexed downward by up to ~2.5 km beneath the seamount. The flexure can be explained by an elastic plate model in which the seamount emplaced upon oceanic lithosphere that was ~10 Myr at the time of loading. Intra-crustal magmatic intrusion may be a feature of hotspot volcanism at young, hot, oceanic lithosphere, whereas, magmatic underplating below a pre-existing Moho may be more likely to occur where a hotspot interacts with oceanic lithosphere that is several tens of millions of years old.

1. Introduction

Oceanic hotspots are associated with active volcanism, a seamount trail that progressively increases age away from the hotspot, and a mid-plate topographic swell. The crust and upper mantle structure above hotspots is the product of the transfer of magmatic material from a deep mantle plume to the Earth's surface. Plume models allow the prediction of melt composition and suggest that the seismic structure of the crust and upper mantle reflects the magmatic "pulse" of a hotspot (White and McKenzie, 1989; Kelemen and Holbrook, 1995). In addition, oceanic volcanoes represent large loads on the lithosphere that deform under their weight (Watts et al., 1985, 1997) and so can be used to study the long-term thermal and mechanical properties of the lithosphere.

The Louisville Ridge (LR) is a major Pacific hotspot track composed of basaltic seamounts formed while the Pacific plate moved over a hotspot, presently located near the intersection of the Eltanin Fracture Zone and the SW Pacific–Antarctica Ridge (Lonslade, 1986; Watts et al., 1988) (Fig. 1). Subduction of the Pacific plate beneath the Indo-Australian plate is causing the north-western end of the LR to collide with the Tonga trench at ~25.8°S. Radiometric age dating of dredge rocks suggests seamount ages of 80–60 Ma for the north-western end of the LR (Koppers et al., 2004). The seafloor that underlies the LR was formed at the Osbourn Trough (OT), a slow-spreading ridge, which ceased spreading during Chron C34, prior to 93 or 87 Ma (Downey et al., 2008). The OT is probably an intra-oceanic rift within the spreading system that rifted apart the Manihiki and Hikurangi Plateaus during the Cretaceous.

In order to determine the crust and upper mantle structure associated with the LR hotspot, we carried out a wide-angle seismic refraction experiment in February 2008 during cruise SO195b of R/V SONNE (Fig. 1). The main aim of the experiment was to determine the relative contribution of magmatism and lithospheric flexure to the crust and upper mantle structure of the LR. Results reveal new insights into how hotspot-generated seamounts build up on the seafloor and how magmatic material is transferred from a deep mantle plume to an overlying lithospheric plate. In addition, we used a seismic and density model to constrain the elastic thickness, T_e, of the lithosphere beneath the Louisville Ridge and hence estimate the age of the underlying oceanic crust.

2. Seismic structure of the Louisville hotspot chain

2.1. Seismic data

We acquired a wide-angle seismic refraction profile P03 along a 340 km long transect that intersects the LR at ~27.6°S (Fig. 1). A total of 31 ocean-bottom-hydrophones or seismometers (OBH/S) recorded

* Corresponding author. Departamento de Geofísica, Universidad de Chile, Blanco Encalada 2002, Santiago, Chile. Tel.: +56 2 978 4296; fax: +56 2 6968686.
E-mail address: econtreras@dgf.uchile.cl (E. Contreras-Reyes).

0012-821X/$ – see front matter © 2009 Elsevier B.V. All rights reserved.
doi:10.1016/j.epsl.2009.11.020

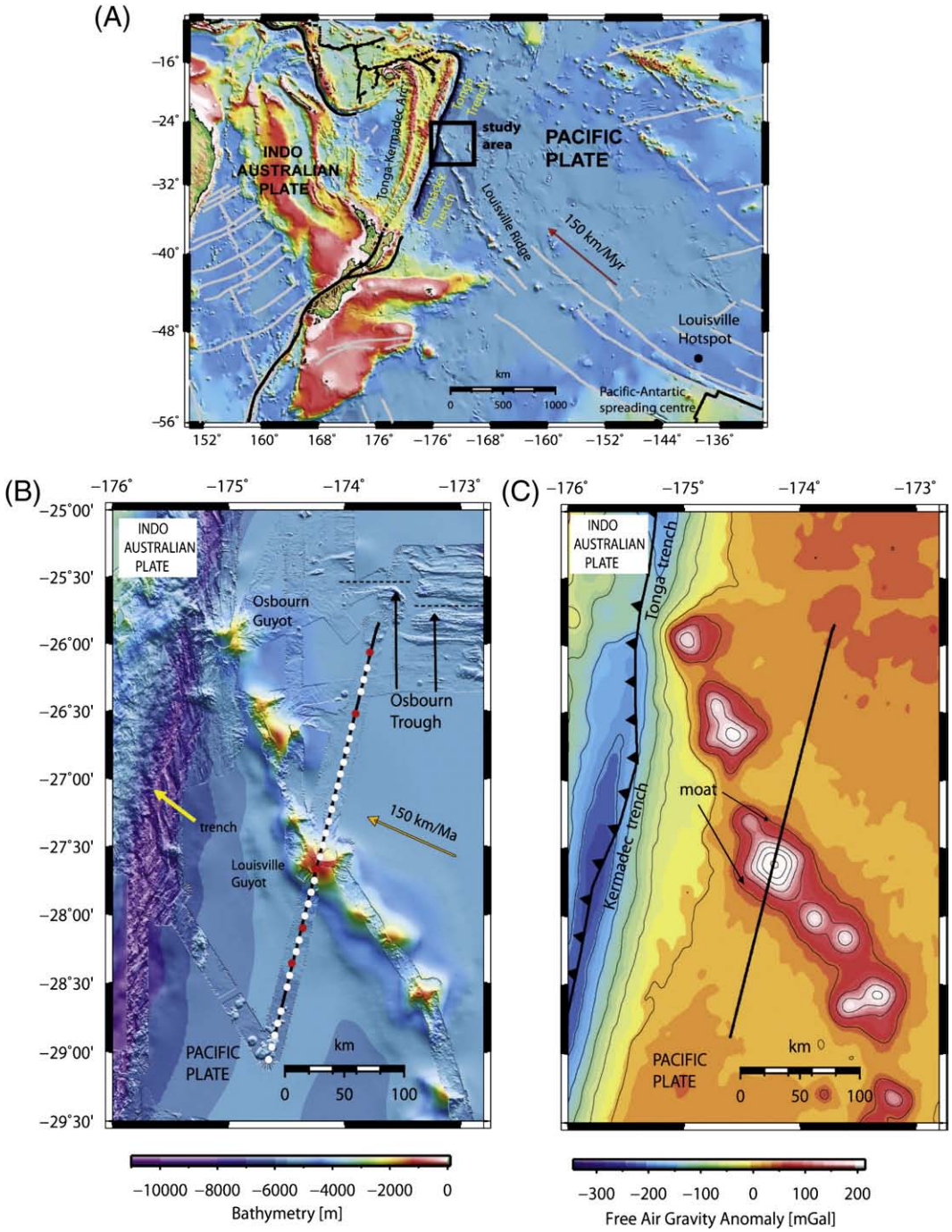

Fig. 1. (A) Tectonic setting showing the Pacific and Indo-Australian plates. The Louisville Ridge is a ~8000 km long volcanic chain of seamounts that formed at a hotspot presently located near the intersection of the Eltanin Fracture Zone with the SW Pacific–Antarctica Ridge (Lonslade, 1986; Watts et al., 1988). (B) Bathymetric map based on GEBCO and swath bathymetric data (Koppers, pers. com) of Pacific plate and westernmost portion of the Louisville hotspot track. The Pacific plate approaches the Tonga-Kermadec trench at a convergence rate of 150 km/Myr (Lonslade, 1986). The axial valleys of the extinct Osbourn Trough spreading centre are shown, together with the location of wide-angle seismic and shipboard gravity profile (black line) used for models in Figs. 4 and 6, respectively. Red dots indicate the five stations (54, 43, 36, 33 and 29) shown in Fig. 2. (C) Satellite derived gravity map over the Tonga trench and the Louisville hotspot track (Sandwell and Smith, 1997). The Louisville Ridge shows the typical free-air gravity anomaly patters associated with flexure due to volcano loading with a high over the ridge and lows in flanking regions. (For interpretation of the references to color in this figure legend, the reader is referred to the web version of this article.)

shots from a G-gun array with a volume of 81 l fired at 60 s time intervals. We recorded intra-crustal refractions (P_g), Moho reflections (P_mP), and upper-mantle refractions (P_n) of excellent quality (Fig. 2). Fig. 2 shows five representative examples of seismic record sections including the identified seismic phases and the predicted travel times based on the final model shown in Fig. 4A. A striking feature of our data is the long offset of both crustal and mantle refractions (>100 km) which enable the detailed structure of the volcanic edifice, oceanic crust and the uppermost ~10 km of the mantle to be determined. Previous studies of other submarine volcanic edifices report reflections from both the pre-hotspot Moho (P_mP) and the base of an underplated body or post-hotspot Moho reflections (Caress et al., 1995; Grevemeyer et al., 2001a). Our seismic data, however, are characterized by a very simple wavefield with a single extraordinarily sharp Moho reflection and a strong mantle refraction (Fig. 2), which suggests the absence of a sub-crustal underplated body.

2.2. Travel-time tomography scheme

We used the inversion method of Korenaga et al. (2000) which allows the joint inversion of seismic refraction and reflection travel time data for a 2-D velocity field. Travel times and ray paths are calculated using a hybrid ray-tracing scheme based on the graph method and local ray-bending refinements (van Avendonk et al., 1998). Smoothing constraints using predefined correlation lengths and optimized damping constraints for the model parameters are employed to regularize an iterative linearized inversion.

The velocity model consists of the following "layers", water, sedimentary-infill, oceanic crust and upper oceanic mantle. To derive the velocity depth model, the water depth was taken from the shipboard bathymetry, which remained fixed during the inversion. In order to obtain the velocity structure of the oceanic crust and sedimentary-infill, we inverted P_g phases (first and later arrivals) to their maximum offset and P_mP phases in order to derive the velocity field of the oceanic crust and Moho depth. Thus, crustal velocities and Moho depths remained fixed for the next step of the inversion, where the upper mantle velocities were derived using oceanic P_n arrivals. The applied hybrid approach uses both first and second arrivals to constrain the velocity model, without the need to disregard for example secondary arrivals such as lower crustal P_g phases, which become secondary arrivals where P_n arrivals overtake P_g. Picking of the seismic phases was carried out manually. Picking errors were assumed to be half a period of one arrival, to account for a possible systematic shift in the arrival identification, and were weighted according to the phase quality.

2.3. Reference model and inversion parameters

We prepared the reference model for the tomographic inversion by 1D-modeling the crustal velocity structure of three OBHs, which we consider as the key stations to define the general structure. Fig. 3 shows the locations of the selected stations. The 2-D reference model was obtained by linearly interpolating the velocities of the three 1-D velocity crustal models (Fig. 3A) (e.g., Sallarès et al., 2003). As the mantle phases were omitted for the crustal inversion, the input model still contains lower crustal velocity below the crust–mantle boundary (Fig. 3A) (e.g., Kopp et al., 2003). The initial thickness of the sedimentary unit overlying

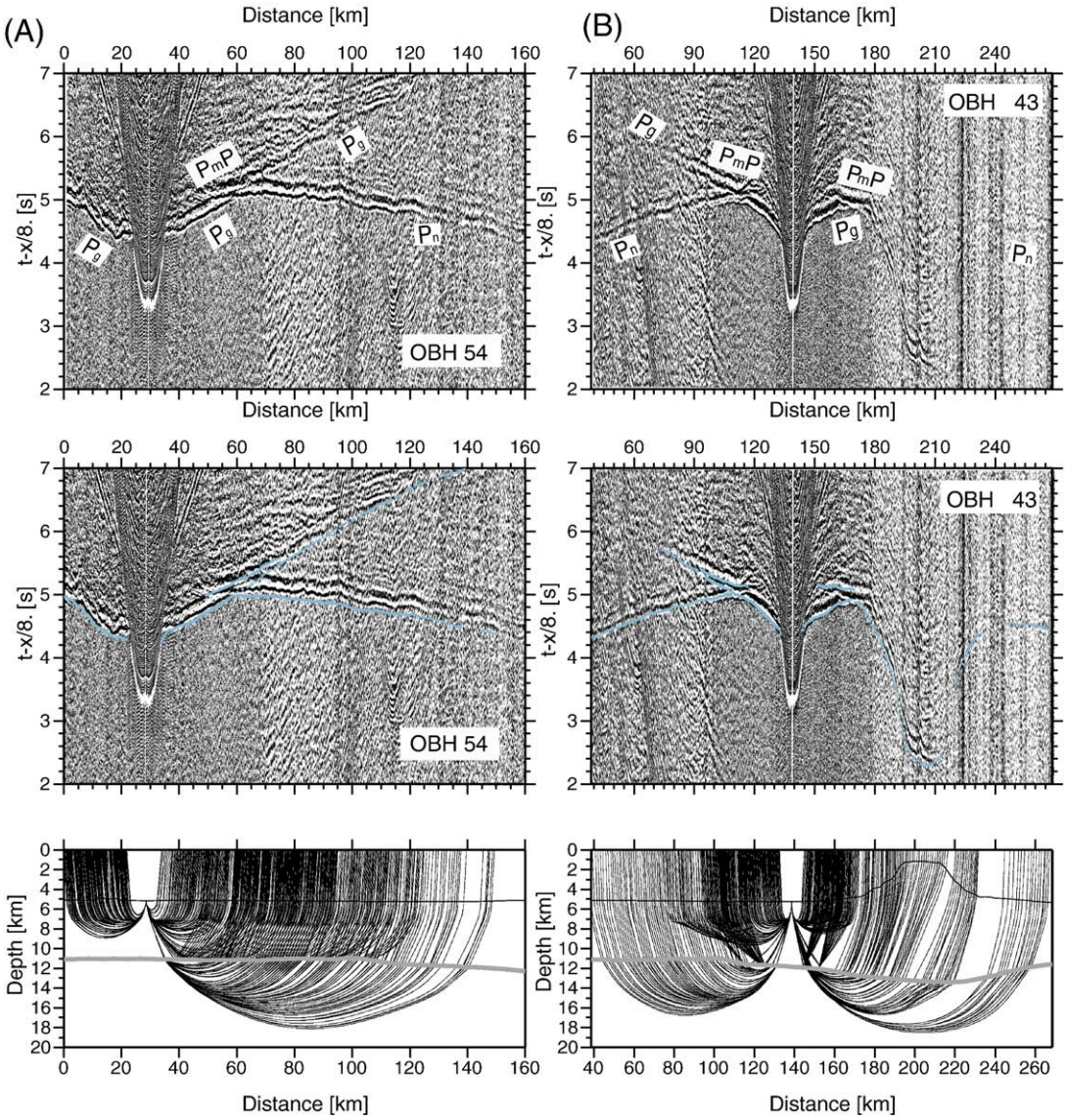

Fig. 2. Examples of wide-angle seismic data with predicted travel times, which are computed based on the velocity model presented in Fig. 4A, and corresponding ray path are also plotted at the bottom. Extremely fast apparent P_n velocities (>8.3 km/s) evidence fast mantle velocities and lack of an underplated subcrustal body. (A) OBH 54, (B) OBH 43, (C) OBH 36, (D) OBH 33 and (E) OBH 29.

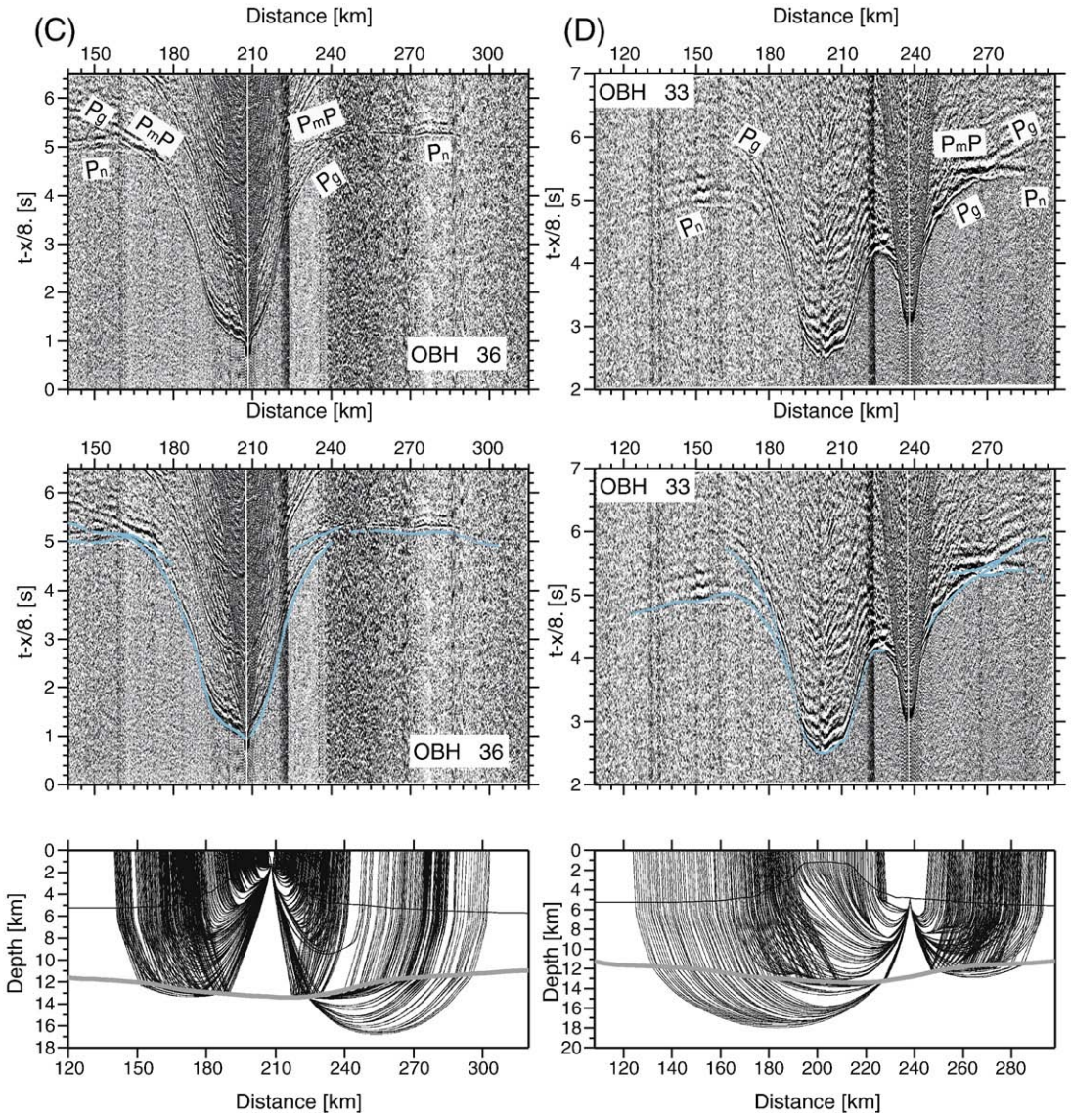

Fig. 2 (*continued*).

the oceanic crust was obtained by picking and converting the vertical incidence reflections from the time migrated seismic reflection data into depths (see Appendix A), using an uppermost velocity of 1.7 km/s and constant velocity gradient of 0.5 km/s/km. We used one floating reflector to model the oceanic Moho. The horizontal grid spacing of the model used for the velocity inversion is 0.5 km, whereas the vertical grid spacing varies from 0.1 km at the top of the model to 1 km at the bottom. We used horizontal correlation lengths ranging from 2 km at the top to 10 km at the bottom of the model, and vertical correlation lengths varying from 0.1 km to 2.5 km, respectively. Different tests showed that varying the values of correlations lengths by 50% does not significantly affect the main features of our models. Because of the trade-off between correlation lengths and smoothing weights, we tried to use shorter correlation lengths and larger smoothing weights in order to reduce memory requirements (Korenaga et al., 2000). Depth and velocity nodes are equally weighted in the refraction and reflection travel time inversions. For a discussion of the velocity-depth ambiguities see Appendix A.

2.4. Uncertainties in the final velocity model

In order to estimate the velocity and Moho depth uncertainties of the final model, we evaluated the effect of randomly perturbed velocities and reflector depths in our reference model upon the tomographic inversion using the Monte Carlo approach (Korenaga et al., 2000). We generated 10 random initial velocity models by adding smooth perturbations randomly distributed (maximum velocity perturbations of ± 0.8 km/s at the top and ± 0.4 km/s at the bottom of the 1D crustal reference models shown in Fig. 3C and D). The initial geometry of the Moho reflector was randomly varied within a range of ± 2 km. In addition to the perturbed reference models we produced 10 so-called noisy arrival time sets constructed by adding random phase errors (± 50 ms) and common receiver errors (± 50 ms) to the original data set (Korenaga et al., 2000). Then we performed a tomographic inversion for each velocity model with one noisy data set (resulting in a total of 100 final models), in order to estimate not only the dependence of the solution on the reference model but also the effect of phase arrival time picking errors. The stopping criterion for each inversion was $\chi^2 < 1$. Fig. 3B shows the average velocity-depth model from the 100 final models.

The standard deviation of the velocities (ΔV) is well constrained in the central portion of the velocity-model with values lower than 0.1 km/s (Fig. 3E). Beneath the seamount, ΔV values in the lower crust increase to values of 0.15 km/s, showing a reduced model resolution. Moho depth uncertainties are higher (± 0.6 km) at the southwestern

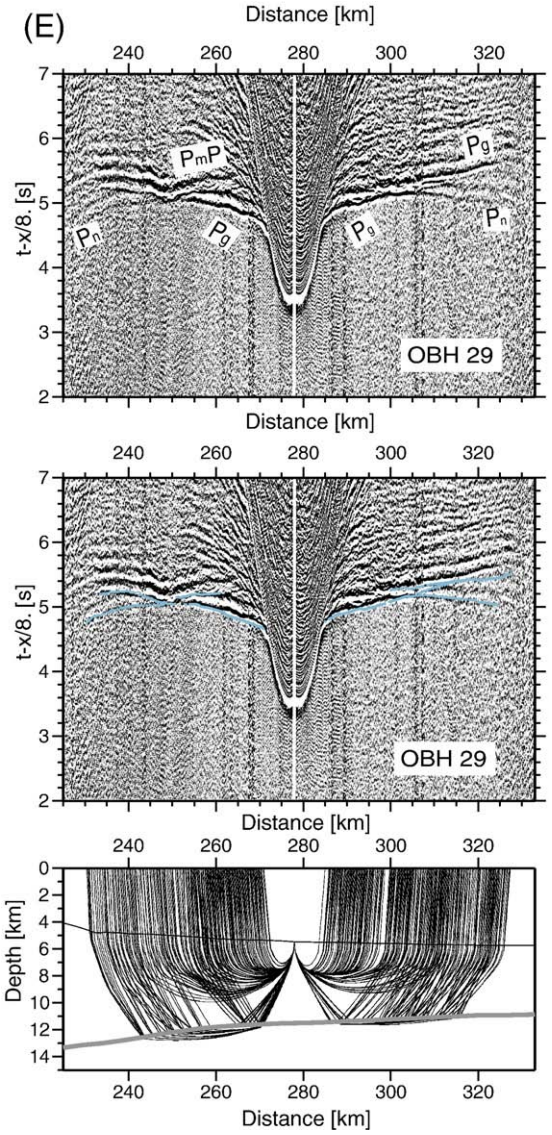

Fig. 2 (*continued*).

edge of the model (Fig. 3E), which is a zone characterized by the absence of P_mP reflections. However, the oceanic Moho is well constrained in the main part of the velocity-depth model (Fig. 3E and F).

For the subsequent tomographic inversion of mantle refractions, a "layer-stripping" procedure was chosen, preserving the structural and velocity information above the Moho interface gained before. Fig. 5A shows the derivative weight sum of all P_n arrivals. Results indicate a high ray density for the upper mantle. For the Monte Carlo approach, we constructed several initial models by varying the uppermost mantle velocity between 7.6 and 8.5 km/s as is shown in Fig. 5B. The final model obtained by averaging the individual Montecarlo solutions, and its uncertainties are plotted in Figs. 4A and 5C, respectively. Upper mantle velocities are well constrained with uncertainties ranging from 0.1 to 0.2 km/s in the resolved upper mantle portions (Fig. 5C).

2.5. Seismic results

The final tomographic model suggests that the Pacific oceanic crust is of normal thickness (5.8 ± 0.3 km) to the northeast and southwest of the volcanic edifice (Fig. 4). Wide-angle P_mP reflections beneath the seamount suggest that the oceanic crust has been flexed downwards by volcano loading, which is consistent with the reduced seismic velocities and free-air gravity anomaly lows (Figs. 1, 4 and 6). The flexural moat that flanks the LR is associated with prominent free-air anomaly lows and is infilled with up to 1–2 km of volcanoclastic material and mass wasting products (e.g., debris flows) derived from individual seamounts along the chain. The infill material is characterized by velocities in the range of 1.6–4.0 km/s. Similar low velocities are associated with the summit region of the seamount, where they may reflect a pelagic drape, hyoclastics or sub-aerial volcanic rocks.

Seismic velocities of the volcanic edifice are generally higher than those observed in the upper crust away from the seamount at equivalent depths (Fig. 4A). We believe these velocities reflect basaltic rocks with a low degree of porosity and fracturing. At ~1.5 km beneath the seamount summit, these velocities transition to high velocities (>6.4–7.2 km/s) which we interpret as mafic intrusive rocks. The high velocities define a symmetrical, semi-conical, shaped core (Fig. 4B) and they suggest that the seamount has built both upwards and outwards. The velocity structure suggests that the volcano has grown dominantly through intrusive, rather than extrusive, processes. Weigel and Grevemeyer (1999) reported similar high velocities (>6.0 km/s) for the core of the Great Meteor seamount but only deeper than 3 km beneath the summit. Zucca et al. (1982) and Canales et al. (2000) have reported velocities of >7 km/s for the intrusive core of the main Island of Hawaii and Tenerife (Canary Islands) respectively, in agreement with our results.

The lowermost oceanic crust shows abnormally fast velocities with values of >7.2–7.6 km/s, suggesting that hotspot volcanism has intruded the pre-existing crust with material characterized by velocities intermediate between mafic lower crust and ultramafic upper mantle. Beneath the edifice and its flanking moat, the mantle is characterized by fast velocities (>8.3 km/s) that reach 8.7 km/s at 7 km mantle-depth (Fig. 4A). Thus, we see no evidence for any high velocity (i.e., >7.2–<8.0 km/s) sub-crustal bodies or underplating of the type described by Watts et al. (1985), Caress et al. (1995), and Charvis et al. (1999) beneath the Hawaiian Islands, Marquesas Islands, and La Reunion respectively.

The relatively fast uppermost mantle velocities of ~8.3 km/s can be attributed to seismic anisotropy in the mantle. Since the seismic transect is oriented approximately orthogonal to the OT spreading centre (Fig. 1B), we would expect that the faster P_n velocity is oriented in that direction (Hess, 1964). Corroborating that, Scherwath et al. (2008) reported P_n velocities of ~7.4 km/s along a trench-perpendicular seismic line at ~29°S, which runs parallel to the OT axis and hence likely matches the orientation of the slow mantle velocity.

3. Gravity model

In order to obtain additional constraints in the structure of the LR, we calculated the gravity effect of the seismic model and compared it to the observed free-air gravity anomaly. Our 2D gravity calculation is based on Parker's (1972) spectral method (see Korenaga et al. (2001) for details). We converted velocity (V) to density (ρ) using the following relationships:

Nafe and Drake (1963) relationship for the sedimentary section,

$$\rho = 1.75 + 0.16V,$$

Carlson and Herrick (1990) relationship for igneous upper crust,

$$\rho = 3.61 - 6.0 / V.$$

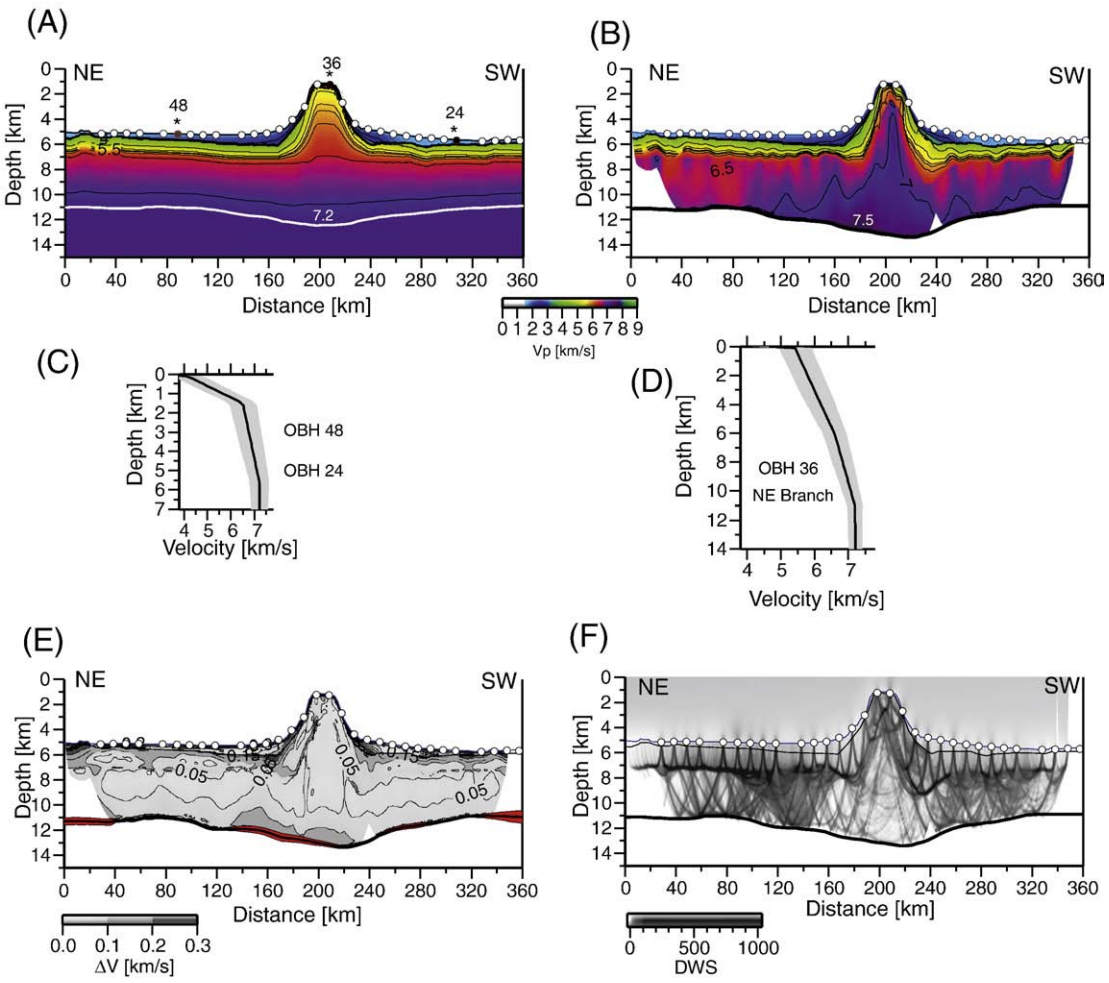

Fig. 3. Result of crustal tomographic inversion using P_g and P_mP phases. (A) Initial velocity model used as a reference for the Monte Carlo analysis and for velocity inversion. (B) Final velocity model derived by averaging all Monte Carlo ensembles. One-dimensional reference models beneath stations 48, 24 (C) and 36 (D) used for the interpolated 2D reference model shown in A. (E) Corresponding standard deviation for velocity and depth nodes (red area), contour interval is at 0.05 km/s. (F) Derivative Weight Sum (DWS) for rays traveling throughout model shown in B. (For interpretation of the references to color in this figure legend, the reader is referred to the web version of this article.)

Birch (1961) law for plagioclase, and diabase-gabbro ecoglite (lower crust),

$$\rho = 0.375(1 + V).$$

Mantle density was kept and assumed to be 3300 kg/m^3. Fig. 6A shows the observed and predicted calculated free-air gravity anomaly obtained by using the derived density model shown in Fig. 6B. The calculated gravity effect of the seismic model fits the gravity data well, and the misfit is smaller than 7 mGal along most of the transect. The best fitting densities of the volcanic load, infill material, oceanic crust and mantle densities are 3000, 2500, 2800 and 3300 kg/m^3, respectively.

Since the density model was derived using analytical velocity-density relationships we can directly compute the density uncertainties $\Delta\rho$ from the velocity uncertainties ΔV trough:

for the sedimentary section,

$$\Delta\rho = 0.16\Delta V,$$

for igneous upper crust,

$$\Delta\rho = 6.0\Delta V / V^2,$$

for lower crust,

$$\Delta\rho = 0.375\Delta V.$$

The density uncertainty model is shown in Fig. 6C. The highest values are found in the upper crust and in the region of high lowermost crustal velocities where $30<\Delta\rho<80$ kg/m^3. Additionally, we test a linear regression for lower crustal rocks of the form $\rho=(V+a)/b$, keeping unchanged the upper crust and sedimentary density structures in order to study the sensibility of the gravity anomaly due to crust density uncertainties. Thus, we set the upper/lower crust boundary to 2800 kg/m^3 and we test different values of a and b in order to vary the lowermost density (ρ_{lc}) between values of 2900 and 3100 kg/m^3. Fig. 6A shows the results using $\rho_{lc}=2900$, 3000 and 3100 kg/m^3. The best fit is reached with 3000 kg/m^3, which is clearly higher than typical gabbro density (~2800 kg/m^3) and much lower than mantle density (~3300 kg/m^3). Therefore we can conclude that seismically constrained high lower crustal velocities under the seamount are in accord with the gravity anomaly data.

4. Flexure of the lithosphere

The LR represents a load on the oceanic lithosphere that should flex under its weight and so it is useful to also compare the seismically constrained Moho depths to predictions based on elastic plate models. We have used a fast Fourier transform technique to calculate the flexure

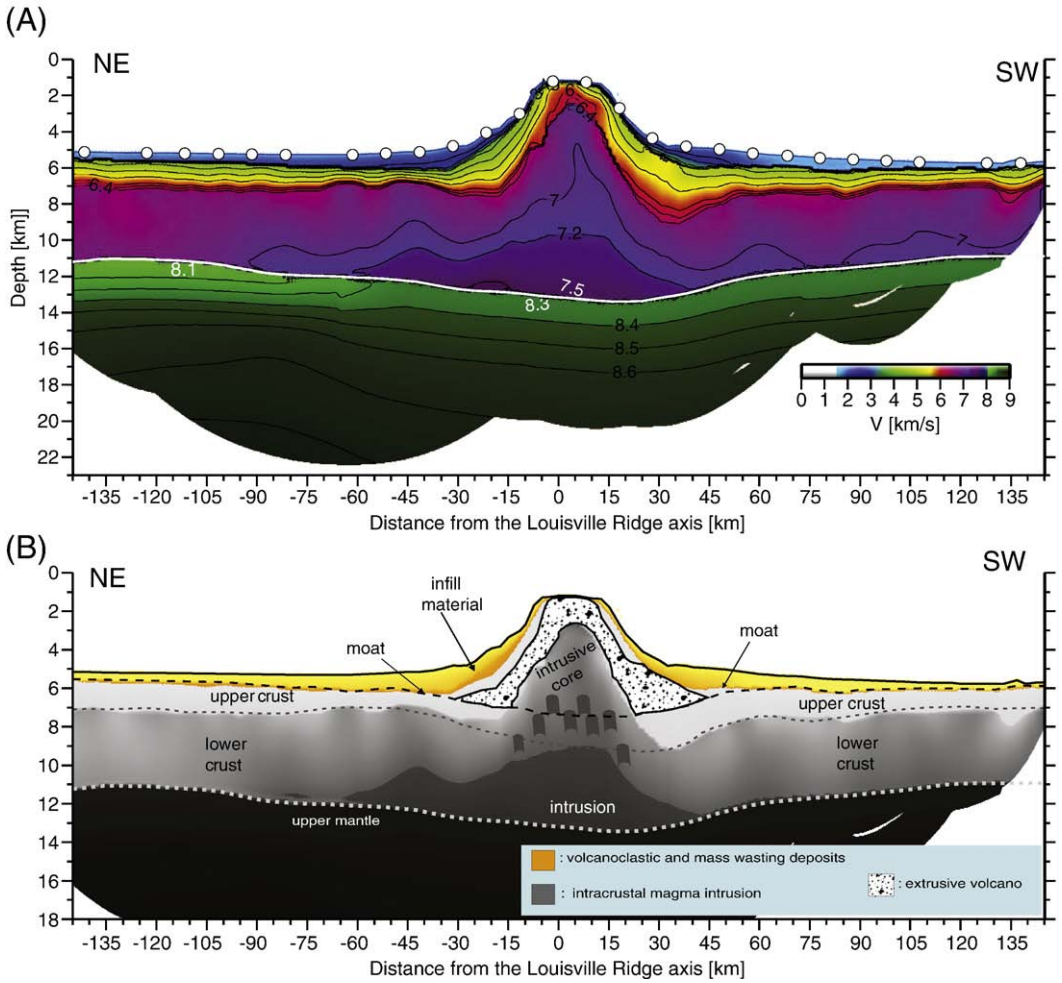

Fig. 4. (A): Velocity model obtained from tomographic inversion of travel times from crustal and mantle phases. The root mean square travel time residuals (TRMS) obtained with the 2-D final model were ~50 ms for crustal phases ($P_g + P_mP$) and ~51 ms for mantle phases. (B): Interpretation based on the detailed tomographic model. Geological structures are based on the following seismic velocities values: >1.5–4.0 km/s for volcanoclastic and mass wasting deposits; >7.2–7.6 km/s for intracrustal magma intrusion; >8.0 km/s for the upper mantle; 5.0–6.4 km/s for the extrusive volcano; and >6.4–7.0 km/s for the intrusive core. Assumed upper and lower crustal velocity ranges are 4.0–6.4 km/s and >6.4–7.2 km/s, respectively.

(e.g., Watts, 1994) and assumed a 5.8 km thick oceanic crust and a constant elastic thickness, T_e, for the Pacific lithosphere. Densities of the volcanic load (3000 kg/m^3), infill material (2500 kg/m^3), and mantle (3300 kg/m^3) were derived from the seismic model. In order to calculate the volcano load we used a median filter (width = 400 km) to remove the outer topographic rise seaward of the Tonga trench from the observed GEBCO 2×2 minute bathymetry. The flexure due to the load was calculated for a range of elastic thickness values ($5 < T_e < 15$ km) and we found that $T_e = 10 \pm 2$ km described the change in seismic Moho depth with an average root mean square misfit (RMS) similar to the Moho depth uncertainties (Fig. 7A).

The flexure models in Fig. 7 depend, of course, on the parameters assumed for the densities of the load, infill and mantle. The load density is of particular importance and large uncertainties in this parameter can lead to large uncertainties in the resulting flexure and, hence, estimate of T_e (e.g., Watts, 1994; Minshull and Charvis, 2001). However, the uncertainties can be significantly reduced by using combined seismic and gravity modeling constraints since there is strong correlation between seismic velocity and density (Carlson and Herrick, 1990).

In order to demonstrate the "trade-off" between volcanic load density and elastic thickness we compare the seismic Moho reflector with the predicted flexed Moho due to different load densities ranging from 2700 to 3100 kg/m^3 at $T_e = 5$, 10 and 15 km. Fig. 7B shows the Moho deflection envelope at $T_e = 10$ km for the mentioned range of load densities. The results show that the predicted flexed Moho depths are comparable to the seismic Moho depths within their uncertainties, which implies that independent of the load density $T_e = 10$ km is a good approximation and it is consistent with the seismic data. In fact, envelopes associated to the crustal flexure at the range of load densities (2700–3100 kg/m^3) with $T_e = 5$ and 15 km shown in Fig. 7C shows an evident mismatch with the seismic Moho even taken in to account the Moho depth uncertainties. $T_e = 5$ km produce too much flexure and $T_e = 15$ km too little (Fig. 7C). Thus, we conclude that $T_e = 10 \pm 2$ km best described the measured change in seismic Moho depth.

Our estimate of T_e is lower than that derived by Lyons et al. (2000) and Watts et al. (2006) using gravitational admittance and predicted bathymetry ($27 < T_e < 29$ km). One possibility is that their values reflect the T_e structure of the outer rise, rather than the LR. Indeed, the age of the oceanic crust that underlied the LR suggests that it should be associated with T_e~25–30 km, although this may be reduced somewhat by yielding in the seaward wall of the Tonga-Kermadec trench (Billen and Gurnis, 2005). If we assume that the relationship between T_e and age of the oceanic lithosphere at the time of loading is described by the depth to the 450 °C oceanic isotherm (Watts, 1978) and that the age of the northern LR is 80–60 Ma (Koppers et al., 2004), this suggests that the age of the crust beneath the LR is ~90–80 Ma. This is generally consistent with the age

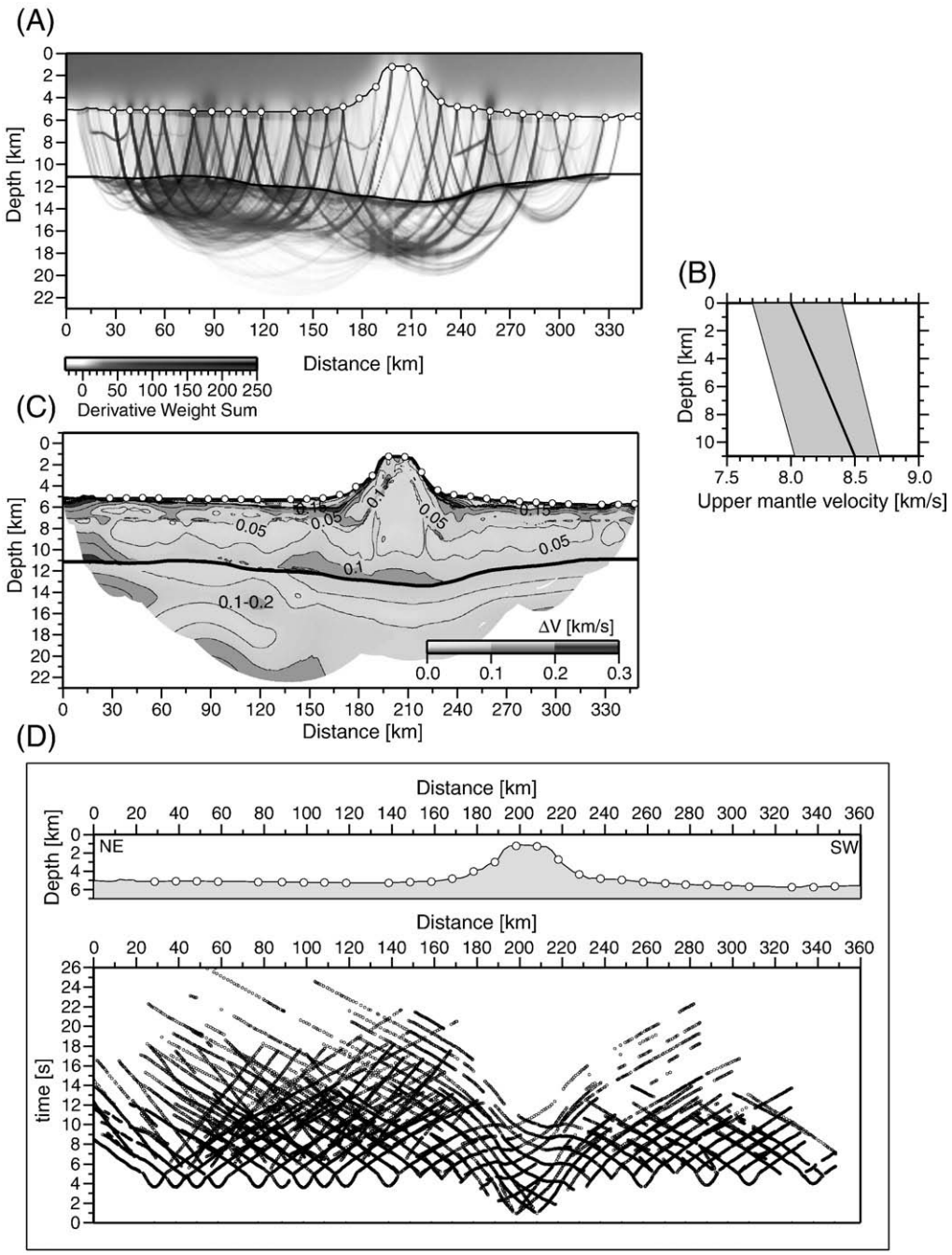

Fig. 5. (A) Derivative Weight Sum (DWS) for rays traveling throughout model shown in Fig. 4A. (B): Reference 1D mantle velocity model measured from the seismic Moho which is used as a reference for the Monte Carlo analysis. (C): Velocity uncertainty model after Monte Carlo type realizations. (D): Travel time picks used for the tomographic inversions and the respective source-receiver geometry and bathymetry of the experiment. More than 12,000 crustal (P_g and P_mP) and 4800 mantle P_n arrivals were picked and inverted to derived the detailed tomographic model shown in Fig. 4A.

proposed by Billen and Stock (2000) and Downey et al. (2008) who suggest that spreading at the OT had ceased by ~84 Ma.

5. Discussion and conclusions

5.1. Volcanic edifice structure

The amount of volcanic material that has been added to the surface of the oceanic crust and intruded into the crust can be estimated by calculating the volume of the volcanic edifice, infill and flexural root. We follow the standard seismic definitions of Houtz and Ewing (1976) which set seismic velocities in the range of 4.0–<6.6 km/s and >6.5–<7.5 km/s to the extrusive-upper and intrusive-lower oceanic layer, respectively. This classification implies that ~60% of the Louisville volcanic edifice is associated to a high-density intrusive core and only the outer ~1.5 km layer corresponds to extrusive high-porosity rocks (Fig. 4). This result is similar to those found by Zucca et al. (1982) and Canales et al. (2000) with volcanic edifice velocities >7.0 km/s for the main Island of Hawaii and Tenerife (Canary Islands), respectively, which were interpreted to be intrusive plutonic complexes. In contrast, other seamounts imaged by seismic refraction data do not present evidence from *P* wave velocity structure of any intrusives such as Marquesas and Tenerife which is

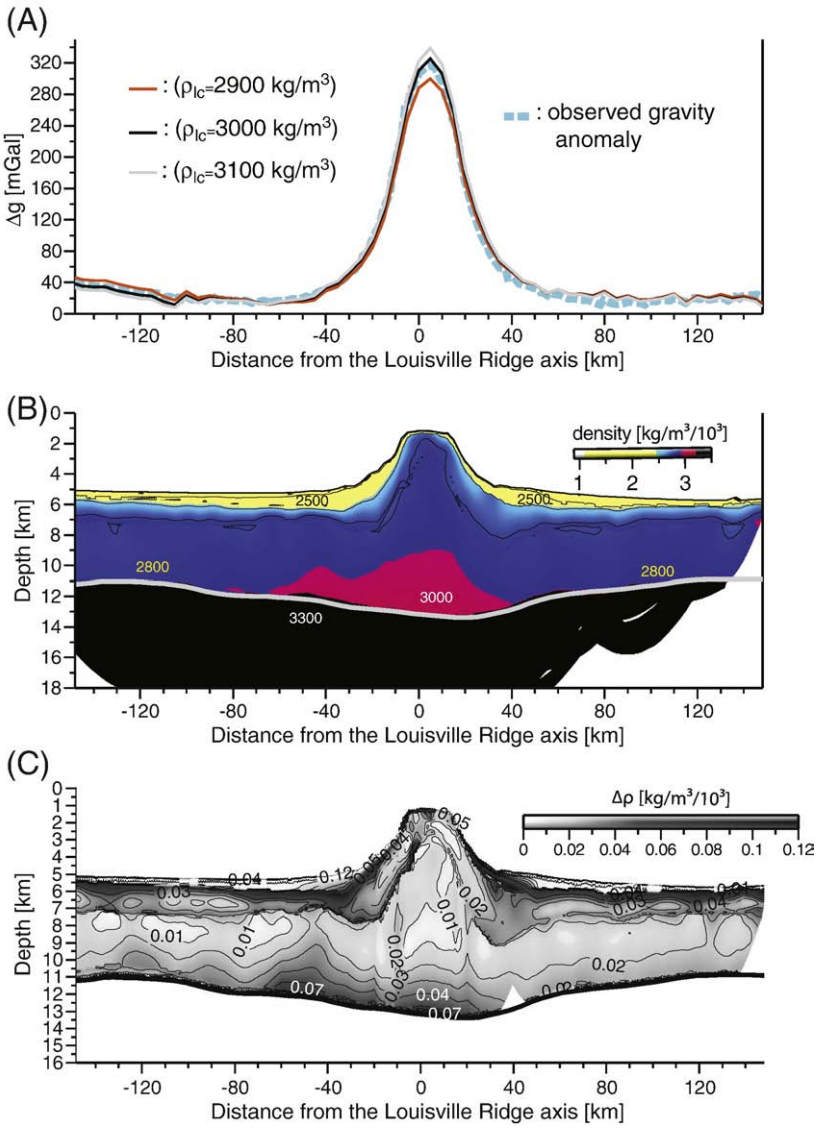

Fig. 6. (A): Dotted blue-light and black lines are the observed and predicted free air gravity anomaly (Δg), respectively. The average root mean square (RMS) residual anomaly is less than 7 mGal. Also we plotted the predicted free air gravity anomaly with lower crustal densities of 2900 kg/m^3 (red line) and 3100 kg/m^3 (gray line) immediately beneath the seamount. The best fit is reached with lower crustal densities of 3000 kg/m^3 (black line) indicative of possible magmatic intrusion into the crust. (B): Preferred density model obtained by converting the velocities to densities. (C): Density uncertainty model obtained from the velocity uncertainty model shown in Fig. 3E. (For interpretation of the references to color in this figure legend, the reader is referred to the web version of this article.)

indicated by the fact that the 6.0 km/s iso-velocity contour is not elevated beneath the volcano, but is either flat or depressed downwards (Watts et al., 1997).

Using the seismic information shown in Fig. 4 we estimate a total volume of 0.17×10^5 km^3 for the magmatic material that has been trapped in the Pacific oceanic crust and intrusive core, whereas the extrusive volume composed of the outer extrusive layer and volcano deposits (infill material) is about 0.38×10^4 km^3. That is, the intrusive/extrusive ratio is as high as ~4.5. This finding reveals that the volcano has grown mainly by intrusive processes and that a much greater amount of magmatic material provided by the hotspot plume has intruded the oceanic crust than has been erupted onto the surface of the crust.

Hammer et al. (1994) studied the seismic structure of Jasper seamount, a small submarine volcano (~3.5 km high) that maybe part of a hotspot generated chain of seamounts 500 km West of Baja, California, and they imaged slow seismic velocities compared to those observed in typical oceanic crust at equivalent subbasement depths. This suggests that the seamount is constructed predominantly of extrusive lavas with high average porosity. Hammer et al. (1994) proposed that seamount size controls the intrusive/extrusive ratio pointing out that Jasper seamount is far smaller than Hawaii, yet both volcanoes exhibit an outer extrusive layer of similar thickness. However, our new results suggest a seamount formed mainly by intrusive processes despite the LR being far smaller than Hawaii. We therefore conclude that the size of a seamount is not a necessary condition controlling the extrusive/intrusive ratio.

5.2. Intra-crustal intrusion versus magmatic underplating

Previous seismic studies of hotspot generated volcanic seamounts and oceanic islands have revealed velocities that are intermediate between typical lower crustal and upper mantle values and therefore that magmatic material may have either ponded beneath or intruded the base of the oceanic crust (e.g. Caress et al., 1995; Grevemeyer et al., 2001a). The high-magnesium basalts generated from abnormally hot mantle, for example, typically exhibit high crustal densities and velocities when they crystallize (White and McKenzie, 1989; Kelemen

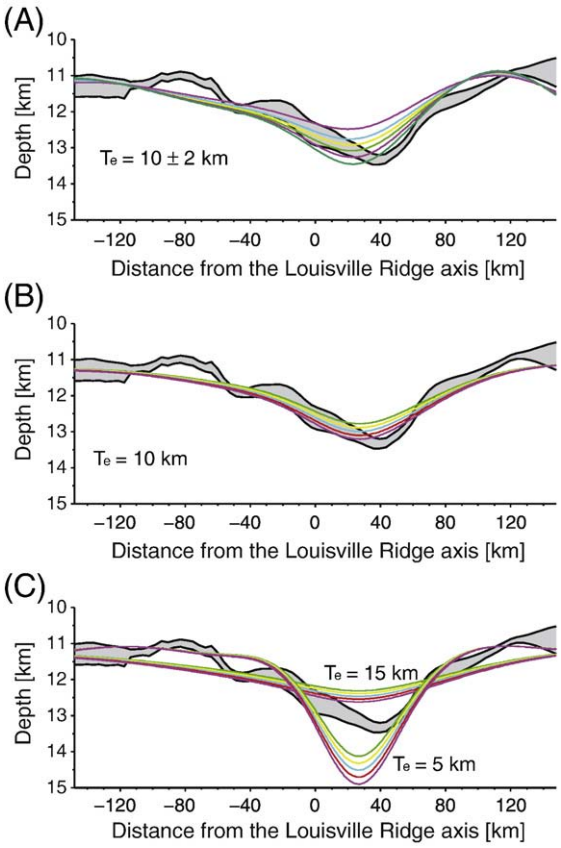

Fig. 7. (A): Comparison between the seismic and flexed Moho using an elastic thickness ranging from 5 to 15 km. Gray area denote the Moho depth uncertainties. $T_e = 10 \pm 2$ km fit the seismic Moho with a RMS misfit comparable to the Moho depth uncertainties. (B): Comparison between the seismic and flexed Moho using an elastic thickness of 10 km and load crustal densities of 2700, 2800, 2900, 3000 and 3100 kg/m^3. Gray area denote the Moho depth uncertainties. (C): Same as (B) but with elastic thickness of 5 and 15 km. Those solutions fail to predict the seismic Moho even if one takes into account the Moho depth uncertainties.

and Holbrook, 1995). Velocities intermediate between lower crustal and upper mantle rocks, interpreted as magmatic underplate have been proposed beneath the Hawaiian and Marquesas islands (e.g. Watts et al., 1985; ten Brink and Brocher, 1987; Caress et al., 1995; Charvis et al., 1999). Other seamounts and oceanic islands, however, do not appear to be underplated (Operto and Charvis 1996; Watts et al., 1997; Grevemeyer et al., 2001b). At the LR, our seismic data reveal much higher mantle velocities (>8.3 km/s) than are typical of underplated seamounts. However, our high lower crustal velocities (7.2–7.6 km/s) suggest that magmatic intrusion is occurring in an intra-crustal rather than a sub-crustal setting. Similarly, recent seismic refraction data at the Hatton Bank and Faroe rifted volcanic margins (White et al., 2008) suggest magmatic bodies that have intruded the lower part of the extended continental crust as sills rather than as an "underplate" of 100% melt.

We believe that the oceanic crust underlying the LR is heavily intruded, because we could not trace a seismic boundary separating the base of the volcanic edifice from the top of the original crust (Fig. 4). Caress et al. (1995) reported high lower crustal velocities (>7.2–7.6 km/s) and low upper mantle velocities (>7.7–8.0 km/s) beneath the Marquesas Islands. The upper crust, however, does not appear to have been intruded. Our new seismic data, in contrast, show magma penetration in both the upper and lower crust, but no melt accumulation in the uppermost mantle below Moho.

The transition from the crust to the mantle is marked in our seismic data by a step in velocity and, hence, density. Unlike other hotspot provinces such as Hawaii and the Marqueses, where seismic imaging has detected the presence of magmatic underplating that lies largely beneath the oceanic Moho, our study of the Louisville Ridge seamount reveals intruded material that lies above the Moho and has seismic velocities more characteristic of the lower oceanic crust. Although developing a more detailed model of the magmatic processes responsible for the Louisville intrusive body is beyond the scope of this study, we are able to speculate here regarding possible explanations.

The seamounts that comprise the northern end of the LR formed on relatively young oceanic crust, and hence the primary mantle melts rose through relatively thin, weak, lithosphere, as compared with the Hawaiian and Marqueses cases, where volcanic edifices were constructed on much older lithosphere of age ~80 Ma and ~40 Ma, respectively. Thus it is possible that a weaker plate facilitated shallower penetration of mantle melts beneath the locus of volcanic extrusion. For example, old, cold and rigid oceanic lithosphere may act to hinder intra-crustal melt penetration, while young, hot and weak lithosphere may allow it (Pollack et al., 1981). The flexural strength depends on the elastic thickness which, in turn, depends upon the thermal age of the lithosphere at the time of volcano emplacement (e.g., Watts, 1978; Calmant et al., 1990). Our estimated elastic thickness suggests the LR formed on a relative young (~10 Myr), hot and thin lithosphere. Perhaps young, hot and thin lithosphere beneath the LR is more vulnerable to magma intrusion than old lithosphere.

By the same token, it is also possible that hot material associated with the Louisville plume was able to rise to relatively shallow depths beneath the oceanic Moho, resulting in lower final pressures of equilibration between melt and residual mantle, and hence lower melt densities (see, e.g., Farnetani et al., 1996). Relatively buoyant primary melt derived from, say, 5–10 km depth, would, upon crystallization, exhibit densities similar to or slightly greater than gabbro, and hence rise naturally above the oceanic Moho. Melts derived from deeper melting, say at 50–150 km depth, would be much more magnesium-rich, with densities intermediate between normal mantle and crustal values, and hence would pond beneath rather than penetrate the Moho. In this way both the temperature and depth of melting in the source plume material may govern the final disposition of intruded magmas. The Louisville Ridge seamount studied here may therefore represent a case of relatively shallow plume melting beneath a young plate, with relatively buoyant intrusive bodies emplaced above the Moho, rather than at or below the Moho as found elsewhere.

Other oceanic hotspot provinces that have been seismically imaged suggest broad, but not perfect, agreement with the Louisville/Hawaii/Marqueses comparison discussed above (Richards et al., pers. com). Of course, other factors such as plate motion, rheology, thermal rejuvenation and plume flux may also affect the amount of magma that is intruded into the crust or underplated.

Acknowledgments

We thank the captain, crew, and technical staff of MV SONNE cruise SO195b for their help at sea. This work was supported by the German Ministry of Education and Research (BMBF), grant 03G0195A and UK Natural Environmental Research Council (NERC) grant NE/F005318/1. Fruitful discussions with Mark A. Richards are greatly appreciated. We wish to acknowledge the useful comments and suggestions from the editor, Rob van der Hilst, and two anonymous reviewers.

Appendix A. Supplementary data

Supplementary data associated with this article can be found, in the online version, at doi:10.1016/j.epsl.2009.11.020.

References

Billen, M.I., Stock, J., 2000. Morphology and origin of the Osbourn Trough. J. Geophys. Res. 105, 13481–13489.

Billen, M.I., Gurnis, M., 2005. Constraints on subducting plate strength within the Kermadec trench. J. Geophys. Res 110. doi10.1029/2004JB003308.

Birch, F., 1961. The velocity compressional waves in rocks to 10 kilobars, part 2. J. Geophys. Res. 66 (7), 2199–2224.

Calmant, S., Francheteau, J., Cazenave, A., 1990. Elastic layer thickening with age of the oceanic lithosphere: a tool for prediction of the age of volcanoes or oceanic crust. Geophys. J. Int. 100, 59–67.

Canales, J.P., Danobeitia, J.J., Watts, A.B., 2000. Wide-angle seismic constraints on the internal structure of Tenerife, Canary Islands. J. Volcanol. Geotherm. Res. 103, 65–81.

Caress, D.W., McNutt, M.K., Detrick, R.S., Mutter, J.C., 1995. Seismic imaging of hot spot-related crustal underplating beneath the Marquesas islands. Nature 373, 600–603.

Carlson, R.L., Herrick, C.N., 1990. Densities and porosities in the oceanic crust and their variations with depth and age. J. Geophys. Res. 95, 9153–9170.

Charvis, P., et al., 1999. Spatial distribution of hotspot material added to the lithosphere under La Réunion, from wide-angle data. J. Geophys. Res. 104, 2875–2893.

Downey, N.J., Stock, J.M., Clayton, R.W., Cande, S.C., 2008. Correction to "History of the Cretaceous Osbourn spreading center". J. Geohpys. Res. 113, B09102. doi10.1029/2008JB006012.

Farnetani, C., Richards, M.A, Ghiorso, M.S, 1996. Petrological models of magma evolution and deep crustal structure beneath hotspots and flood basalts provinces. Earth planet. Sci. Lett. 143 (1-4), 81–94.

Grevemeyer, I., Flueh, E.R., Reichert, C., Bialas, J., Kläschen, D., Kopp, C., 2001a. Crustal architecture and deep structure of the Ninetyeast Ridge hotspot trail from active-source ocean-bottom seismology. Geophys. J. Int. 144, 414–431.

Grevemeyer, I., Weigel, W., Schuessler, S., Avedic, F., 2001b. Crustal and upper mantle seismic structure and lithospheric flexure along the Society Island hot spot chain. Geophys. J. Int. 137, 123–140.

Hammer, P.T.C., Dorman, L.M., Hildebrand, J.A., Cornuelle, B.D., 1994. Jasper Seamount structure: seafloor seismic refraction tomography. J. Geophys. Res. 99 (B4), 6731–6752.

Hess, H.H., 1964. Seismic anisotropy of the upper mantle under oceans. Nature 23, 629–631.

Houtz, R., Ewing, J., 1976. Upper crustal structure as a function of plate age. J. Geophys. Res. 81, 2490–2498.

Kelemen, P.B., Holbrook, W.S., 1995. Origin of thick, high-velocity igneous crust along the U.S. East Coast Margin. J. Geophys. Res. 100 (B6), 10077–10094.

Kopp, H., Kopp, C., Phipps Morgan, J., Flueh, E.R., Weinrebe, W., Morgan, W.J., 2003. Fossil hot spot-ridge interaction in the Musicians Seamount Province: geophysical investigations of hot spot volcanism at volcanic elongated ridges. J. Geophys. Res. 108 (B3), 2160. doi10.1029/2002JB002015.

Koppers, A.A.P., Duncan, R.A., Steinberger, B., 2004. Implications of a nonlinear $^{40}Ar/^{39}Ar$ age progression along the Louisville seamount trail for models of fixed and moving hot spots. Geochem. Geophys. Geosyst. 5, Q06L02. doi10.1029/2003GC000671.

Korenaga, J., Holbrook, W.S., Kent, G.M., Kelemen, P.B., Detrick, R.S., Larsen, H.C., Hopper, J.R., Dahl-Jensen, T., 2000. Crustal structure of the southeast Greenland margin from joint refraction and reflection seismic tomography. J. Geophys. Res. 105, 21591–21614.

Korenaga, J., Holbrook, W.S., Detrick, S., Kelemen, P.B., 2001. Gravity anomalies and crustal structure at the southeast Greenland margin. J. Geophys. Res. 106, 8853–8870.

Lonslade, P., 1986. A multibeam reconnaissance of the Tonga trench axis and its intersection with the Louisville chain. Mar. Geophys. Res. 8, 295–327.

Lyons, S.N., Sandwell, D.T., Smith, W.H.F., 2000. Three-dimensional estimation of elastic thickness under the Louisville Ridge. J. Geophys. Res. 105 (B6), 13239–13252.

Minshull, T.A., Charvis, P., 2001. Ocean island densities and models of lithospheric flexure. Geophys. J. Int. 145, 731–739.

Nafe, J.E., Drake, C.L., 1963. Physical properties of marine sediments. In: Hill, M.N. (Ed.), The Sea. Wiley-Interscience, New York, pp. 794–815.

Operto, S., Charvis, P., 1996. Deep structure of the southern Kerguelen Plateau (southern Indian Ocean) from ocean bottom seismometer wide-angle seismic data. J. Geophys. Res. 101 (B11), 25077–25103.

Parker, R.L., 1972. The rapid calculation of potential anomalies. Geophys. J. R. Astron. Soc. 31, 447–455.

Pollack, H.N., Gass, I.G., Thorpe, R.S., Chapman, D.S., 1981. On the Vulnerability of Lithospheric Plates to Mid-Plate Volcanism: reply to comments by P.R. Vogt. J. Geophys. Res. 86 (B2), 961–966.

Sallarès, V., Charvis, P., Flueh, E.R., Bialas, J., 2003. Seismic structure of Cocos and Malpelo Volcanic Ridges and implications for hot spot-ridge interaction. J. Geophys. Res. 108 (B12), 2564. doi10.1029/2003JB002431.

Scherwath, M., Kopp, H., Flueh, E.R., Henrys, S.A., Sutherland, R., 2008. Structure and deformation of the Hikurangi–Kermadec subduction zone-transitions revealed by seismic wide-angle data. Fall Meet, Suppl., Abstract T23A-1997: Eos Trans. AGU, vol. 89(52).

Sandwell, D.T., Smith, W.H.F., 1997. Marine gravity anomaly from Geosat and ERS-1 satellite altimetry. J. Geophys. Res. 102, 10039–10054.

Ten Brink, U.S., Brocher, T.M., 1987. Multichannel seismic evidence for a subcrustal intrusive complex under Oahu and a model for Hawaiian volcanism. J. Geophys. Res. 92 (B13), 13687–13707.

van Avendonk, H.J.A., Harding, A.J., Orcutt, J.A., 1998. A two-dimensional tomographic study of the Clipperton transform fault. J. Geophys. Res. 103, 17885–17899.

Watts, A.B., 1978. An analysis of isostasy in the world's oceans 1. Hawaiian-Emperor Seamount Chain. J. Geophys. Res. 83, 5989–6004.

Watts, A.B., ten Brink, U.S., Buhl, P., Brocher, T., 1985. A multichannel seismic study of lithospheric flexure across the Hawaiian-Emperor seamount chain. Nature 315, 105–111.

Watts, A.B., Weissel, J.K., Duncan, R.A, Larson, R.L., 1988. Origin of the Louisville Ridge and its relationship to the Eltanian fracture zone system. J. Geophys. Res. 93, 3051–3077.

Watts, A.B., Peirce, C., Collier, J., Dalwood, R., Canales, J.P., Henstock, T.J., 1997. A seismic study of lithosphere flexure in the vicinity of Tenerife, Canary Islands. Earth Planet. Sci. Lett. 146, 431–447.

Watts, A.B., 1994. Crustal structure, gravity anomalies and flexure of the lithosphere in the vicinity of the Canary Islands. Geophys. J. 119, 648–666.

Watts, A.B., Sandwell, D.T., Smith, W.H.F., Wessel, P., 2006. Global gravity, bathymetry, and the distribution of submarine volcanism through space and time. J. Geophys. Res. 111, B08408. doi10.1029/2005JB004083.

Weigel, W., Grevemeyer, I., 1999. The Great Meteor seamount: seismic structure of a submerged intraplate volcano. J. Geodyn. 28, 27–40.

White, R.S., McKenzie, D.P., 1989. The generation of volcanic continental margins and flood basalts. J. geophys. Res. 94, 7685–7729.

White, R.S., Smith, L.K., Roberts, A.W., Christie, P.A.F., Kusznir, N.J., and the rest of the iSIMM Team, 2008. Lower-crustal intrusion on the North Atlantic continental margin. Nature 452, 460–464. doi10.1038/nature06687.

Zucca, J.J., Hill, D.P., Kovach, R.L., 1982. Crustal structure of Mauna Loa Volcano, Hawaii from seismic refraction and gravity data. Bull. Seismol. Soc. Am. 72, 1535–1550.